An Analog Open-Loop Adaptive-Array Antenna System

YASUTAKA OGAWA, Member, IEEE
MANABU OHMIYA
KIYOHIKO ITOH, Member, IEEE
University of Hokkaido

A new open-loop adaptive-array system with excellent transient behavior is presented. The system is constructed of analog circuits and determines complex weights without using the feedback of the array output.

The performance attainable with the system is described in detail. It is shown that the convergence rate of the system does not depend on a noise environment but is determined by the time constant of the low-pass filters included. Moreover, it is shown that although the steady-state performance is quite good when the interference sources differ widely in signal strength, the steady-state performance can be far below optimum when two or more interference sources are present at roughly equal power levels.

Manuscript received June 4, 1981.

Authors' address: Department of Electronic Engineering, Faculty of Engineering, Hokkaido University, Kita 13, Nishi 8, Kita-Ku, Sapporo 060, Japan.

0018-9251/83/0100-0089 $00.75 © 1983 IEEE

I. INTRODUCTION

Rapid convergence is one of the most important requirements for an adaptive array. Especially, an adaptive array in airborne communication and fast-scanning radar systems must provide a very rapid convergence rate. Conventional closed-loop adaptive arrays [1, 2] based on a gradient technique, however, have two problems regarding the convergence rate. The first is that the convergence condition on a loop gain (or a step size) limits the convergence rate [1, 3]. The second is that the convergence rate depends highly on the noise environment [4, 5]. Therefore it is impossible to estimate the convergence time a priori. The problem limits the dynamic range of the adaptive arrays [5]. In order to find a solution to these problems, several methods which improve the conventional closed-loop systems have been proposed [4, 5].

An SMI algorithm which does not use the gradient technique has been also proposed to solve the above convergence rate problems [6]. The convergence rate of this method is, however, limited by the processing time of each digital logic component. Moreover it is necessary to implement a considerable amount of circuitry to realize a rapid convergence.

In this paper, we present an analog open-loop adaptive-array system which is not based on the gradient technique. The system is constructed of analog circuits. And its weights are obtained directly from input data not using the feedback of the array output. Therefore the system is unconditionally stable and provides a rapid convergence rate. Moreover the convergence rate does not depend on the noise environment. It is determined by the time constant of low-pass filters in the system. The system has a very good steady-state performance when interference sources differ widely in signal strength. The steady-state performance, however, degrades substantially when two or more interference sources are present at roughly equal power levels.

This paper is organized as follows. In Section II we describe the configuration of the analog open-loop adaptive-array system. In Section III, we obtain its steady-state performance. Section IV presents the simulation results which show the transient behavior and the effect of steady-state weight jitter.

II. CONFIGURATION OF ANALOG OPEN-LOOP ADAPTIVE-ARRAY SYSTEMS

This paper deals with linear arrays which contain isotropic elements spaced l apart. We assume that a desired signal, an interference signal, and internal thermal noise are zero-mean ergodic stochastic processes and are statistically independent of each other. We also assume that the thermal noise components on different elements are independent, that the desired signal arrival angle is known, and that the array antenna is adjusted mechanically in such a way that the desired signal is incident on

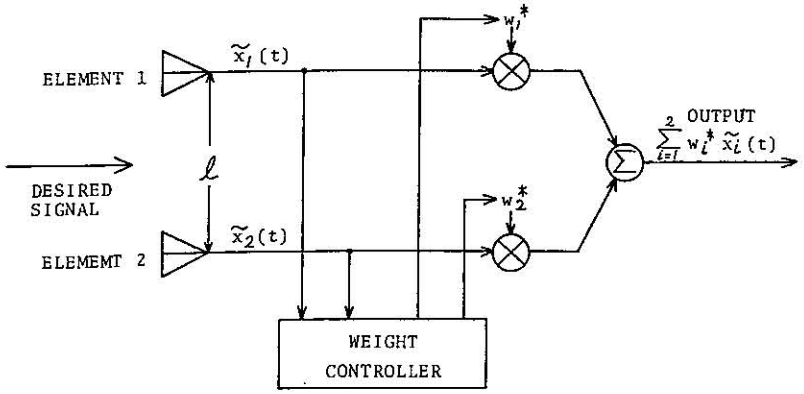

Fig. 1. Single-stage open-loop adaptive-array system.

the array from broadside. Finally, we assume that mutual coupling does not affect the signal from broadside.

A. Single-Stage System

We first treat the two-element adaptive array system shown in Fig. 1. We refer to it as a single-stage system.

From the above assumptions the desired signal is incident on both elements in phase. Then the complex envelope of the desired signal from each array element may be represented by $\tilde{d}(t)$. Let P_d be the desired signal power. Then P_d is given by

$$P_d = \frac{1}{2} < \tilde{d}(t)\, \tilde{d}^*(t) > \tag{1}$$

where $<\bullet>$ and * denote the ensemble average and complex conjugation, respectively.

Let $\tilde{x}_1(t)$ and $\tilde{x}_2(t)$ be the complex envelopes of the signals (the sum of the desired signal, interference signal, and internal thermal noise) from each element. Then defining the covariance matrix by R_{xx}, we have

$$R_{xx} = \frac{1}{2}\begin{bmatrix} <\tilde{x}_1(t)\, \tilde{x}_1^*(t)> & <\tilde{x}_1(t)\, \tilde{x}_2^*(t)> \\ <\tilde{x}_1^*(t)\, \tilde{x}_2(t)> & <\tilde{x}_2(t)\, \tilde{x}_2^*(t)> \end{bmatrix}. \tag{2}$$

We define the covariance matrix of the desired signal components from each element by R_{DD}. Similarly R_{NN} represents the covariance matrix of the noise components (the sum of the interference signal and internal thermal noise). These covariance matrices may be expressed as

$$R_{DD} = \begin{bmatrix} P_d & P_d \\ P_d & P_d \end{bmatrix} \tag{3}$$

$$R_{NN} = \begin{bmatrix} \alpha_1 & \beta \\ \beta^* & \alpha_2 \end{bmatrix} \tag{4}$$

where α_1, α_2, and β are determined by the noise environment.

Because of the statistical independence, the following expression is obtained:

$$R_{xx} = R_{DD} + R_{NN}. \tag{5}$$

Now we define the weight vector consisting of complex weights w_1 and w_2 by $\boldsymbol{W}$. The output SINR (signal to interference plus noise ratio) is given by

$$\text{SINR} = \boldsymbol{W}^\dagger R_{DD}\, \boldsymbol{W} \Big/ \boldsymbol{W}^\dagger R_{NN}\, \boldsymbol{W} \tag{6}$$

where

$$\boldsymbol{W} \triangleq \begin{bmatrix} w_1 \\ w_2 \end{bmatrix} \tag{7}$$

and $\dagger$ denotes Hermitian conjugation.

In this paper we employ the output SINR as a criterion function. We estimate the performance of the system by the output SINR. Representing the eigenvector corresponding to the maximum eigenvalue of $R_{NN}^{-1} R_{DD}$ by $\boldsymbol{U}_{\max}$, the optimum weight vector $\boldsymbol{W}_{\text{opt}}$ which maximizes (6) is given by

$$\boldsymbol{W}_{\text{opt}} = \alpha \boldsymbol{U}_{\max} \tag{8}$$

where a is a nonzero arbitrary complex number.

Obtaining $\boldsymbol{U}_{\max}$ from (3) and (4) and using (2), (5), and (8), $\boldsymbol{W}_{\text{opt}}$ is given by

$$\boldsymbol{W}_{\text{opt}} = \begin{bmatrix} \alpha_2 - \beta \\ \alpha_1 - \beta^* \end{bmatrix} \tag{9}$$

$$= \frac{1}{2}\begin{bmatrix} <\tilde{x}_2(t)\, \tilde{x}_2^*(t)> - <\tilde{x}_1(t)\, \tilde{x}_2^*(t)> \\ <\tilde{x}_1(t)\, \tilde{x}_1^*(t)> - <\tilde{x}_1^*(t)\, \tilde{x}_2(t)> \end{bmatrix}. \tag{10}$$

Because each stochastic process is ergodic, the ensemble average may be replaced by a time average. Then $\boldsymbol{W}_{\text{opt}}$ is expressed as

$$\boldsymbol{W}_{\text{opt}} = \frac{1}{2}\begin{bmatrix} \{\tilde{x}_2(t)\, \tilde{x}_2^*(t)\}_{\text{dc}} - \{\tilde{x}_1(t)\, \tilde{x}_2^*(t)\}_{\text{dc}} \\ \{\tilde{x}_1(t)\, \tilde{x}_1^*(t)\}_{\text{dc}} - \{\tilde{x}_1^*(t)\, \tilde{x}_2(t)\}_{\text{dc}} \end{bmatrix} \tag{11}$$

where $\{b(t)\}_{\text{dc}}$ denotes the dc component of $b(t)$. It is possible to extract the dc component by use of a low-pass filter. Employing a first-order low-pass filter, a single-stage system can be constructed as shown in Fig. 2. As may readily be seen, the system is unconditionally stable and the transient behavior is determined by the time constant τ of the filters. The smaller the time constant, the

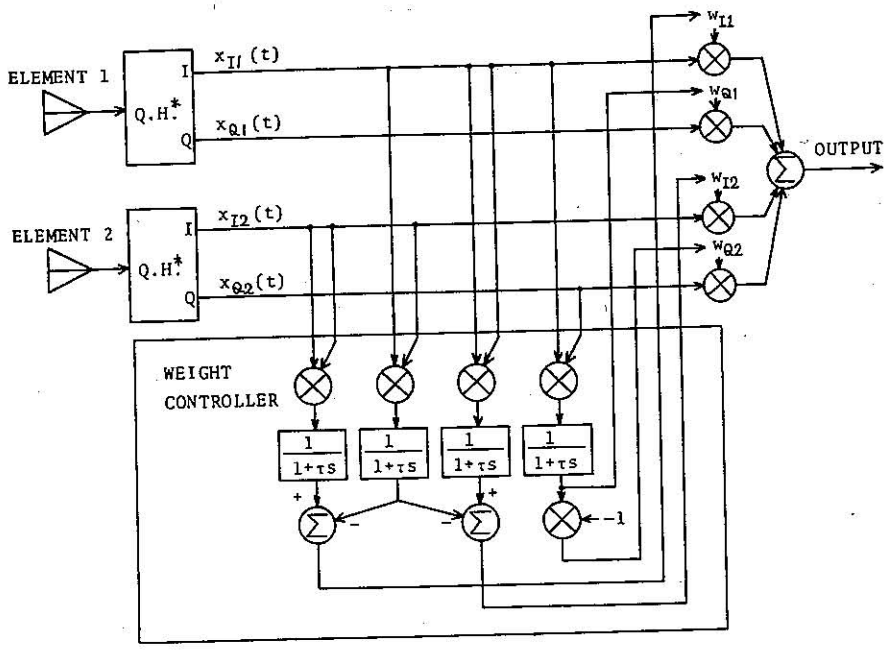

Fig. 2. Single-stage analog open-loop adaptive-array system employing first-order low-pass filters. *indicates quadrature hybrid. $x_{Ik}(t) \triangleq \mathrm{Re}\{\tilde{x}_k(t) \quad e^{j2\pi f_c t}\}$, $x_{Qk}(t) \triangleq \mathrm{Re}\{-j\,\tilde{x}_k(t)\, e^{j2\pi f_c t}\}$, $w_{Ik} \triangleq \mathrm{Re}\{w_k\}$, $w_{Qk} \triangleq \mathrm{Im}\{w_k\}$ $(k=1,2)$.

more rapid the convergence. Too small a time constant, however, causes substantial weight jitter. Unfortunately, general considerations on the relation between the time constant and weight jitter are not yet available. For a specific case, the problem is discussed by using computer simulation results presented in Section IV.

According to (11) the amplitude of the optimum complex weights depends on the interference signal power. Thus it seems that a wide dynamic range of the interference signal power requires that circuit components have a wide dynamic range capability. However the amplitude of the complex weights does not have any effect on the output SINR; only the relative phase is important. Therefore the dynamic range problem may be removed to a considerable extent by improved circuit design. We shall not consider improved circuit design here.

B. Multiple-Stage System

In a case where the adaptive array contains three or more elements, it is practically impossible to realize an open-loop analog weight controller which maximizes the output SINR of the array. This is because the network becomes too complex. Instead, we employ a two-stage Davies cascade [9] for a three-element array as shown in Fig. 3. The configuration of the weight controllers is identical to that described in the previous subsection. Each weight controller determines the complex weights in such a way that the output SINR at each stage is maximized. For example, the weight controller 1 in Fig. 3 determines w_1 and w_2 in such a way as to maximize the SINR of $\tilde{x}_3(t)$ by using $\tilde{x}_1(t)$ and $\tilde{x}_2(t)$. If the array contains more elements, the system may be constructed by increasing stages. The multiple-stage system has the following advantages over the single-stage one.

1) The multiple-stage system has plural independent nulls. Some of them may be formed coincidently. Therefore the multiple-stage system is very tolerant to component errors.

2) The protection capability to a single broadband interference signal is improved significantly as shown in the next section.

3) The multiple-stage system may reduce plural narrowband interference signals when they are widely separated in power level.

The multiple-stage systems, however, do not produce optimum results for multiple interference signals of nearly equal power.

III. STEADY-STATE PERFORMANCE

In this section we discuss the steady-state performance of open-loop systems. We assume throughout the rest of the paper that there are neither component errors nor mutual coupling between array elements. We have $\alpha_1 = \alpha_2$, $\langle \tilde{x}_1(t)\, \tilde{x}_1^*(t)\rangle = \langle \tilde{x}_2(t)\, \tilde{x}_2^*(t)\rangle = \langle \tilde{x}_1'(t)\, \tilde{x}_1'^*(t)\rangle = \langle \tilde{x}_2'(t)\, \tilde{x}_2'^*(t)\rangle$, $\langle \tilde{x}_1(t)\, \tilde{x}_2^*(t)\rangle = \langle \tilde{x}_1'(t)\, \tilde{x}_2'^*(t)\rangle$, and $\langle \tilde{x}_3(t)\, \tilde{x}_3^*(t)\rangle = \langle \tilde{x}_4(t)\, \tilde{x}_4^*(t)\rangle$. Also in this section we assume there is no weight jitter.

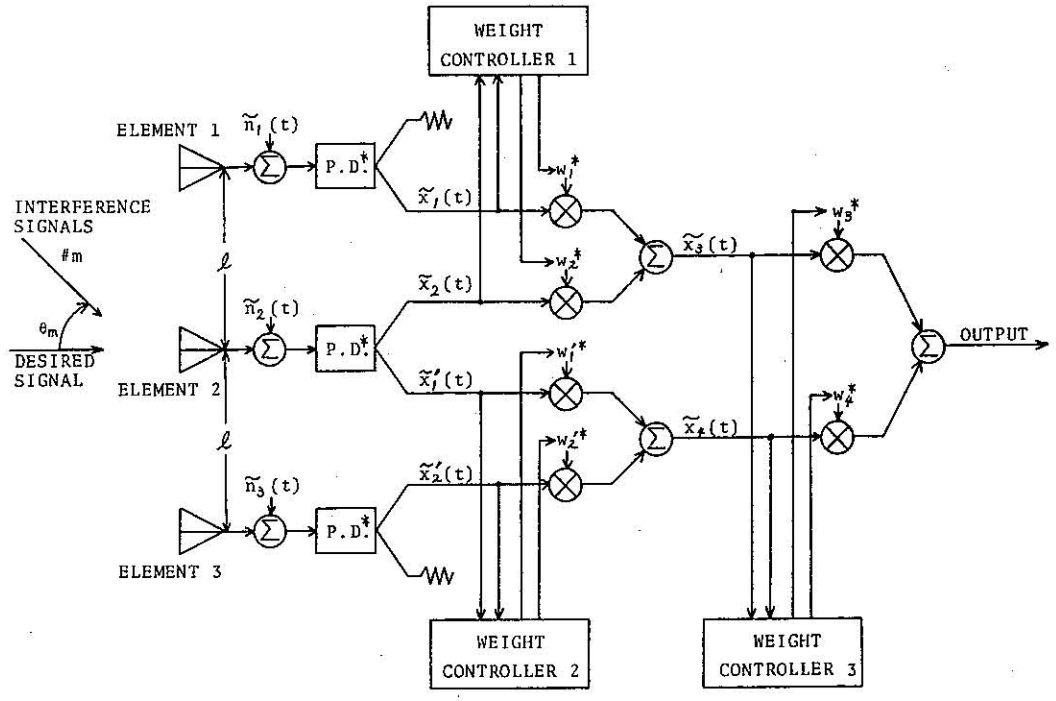

Fig. 3. Two-stage analog open-loop adaptive-array system. * indicates two-way in-phase power dividers.

A. Steady-State Performance of Single-Stage System

Let $\boldsymbol{H}_{DX}$ be the correlation vector between the desired signal $\tilde{d}(t)$ and the signals $\tilde{x}_1(t)$ and $\tilde{x}_2(t)$, i.e.,

$$\boldsymbol{H}_{DX} = \frac{1}{2}\begin{bmatrix} <\tilde{d}^*(t)\,\tilde{x}_1(t)> \\ <\tilde{d}^*(t)\,\tilde{x}_2(t)> \end{bmatrix}. \tag{12}$$

From (1) and the statistical independence of each stochastic process,

$$\boldsymbol{H}_{DX} = \begin{bmatrix} P_d \\ P_d \end{bmatrix} \tag{13}$$

holds.

From (2) and (13) it is seen that the optimum weight $\boldsymbol{W}_{\text{opt}}$ given by (10) is equal to $R_{XX}^{-1}\,\boldsymbol{H}_{DX}$ to within a multiplicative constant. This means that $\boldsymbol{W}_{\text{opt}}$ is identical to the optimum solution given by the least mean square (LMS) algorithm [1]. Consequently the steady-state performance of the single-stage open-loop system is available from the results set forth in [1, 11].

B. Steady-State Performance of Multiple-Stage System

In this subsection we obtain the steady-state performance of the two-stage system shown in Fig. 3. We may readily extend the considerations for a system with more stages. From the assumptions that there are neither component errors nor mutual coupling, $w_1' = w_1$ and $w_2' = w_2$ hold. We consider that M independent interference signals exist in the field. Each interference signal is assumed to arrive from spatial angle θ_m $(m=1,\ldots M)$ relative to a broadside. Let $\tilde{i}_m(t)$ be a complex envelope of the mth interference signal from element 1. Then the complex envelopes from elements 2 and 3 are represented by $\tilde{i}_m(t-t_m)\,e^{-j\phi_m}$ and $\tilde{i}_m(t-2t_m)\,e^{-j2\phi_m}$, respectively. t_m and ϕ_m are defined as follows:

$$t_m \triangleq l \sin\theta_m / c \qquad (m=1,\ldots,M) \tag{14}$$

$$\phi_m \triangleq 2\pi f_c\, t_m \qquad (m=1,\ldots,M) \tag{15}$$

where c is the speed of light and f_c is the center frequency. We represent the power of the mth interference signal by P_{im}. Then we have

$$P_{im} = \frac{1}{2} < \tilde{i}_m(t)\,\tilde{i}_m^*(t) >. \tag{16}$$

For convenience, we assume that the internal thermal noise is added to each channel behind the array element as shown in Fig. 3. Let $\tilde{n}_1(t)$, $\tilde{n}_2(t)$, and $\tilde{n}_3(t)$ denote the complex envelopes of the internal thermal noise components. Then the internal thermal noise power P_n is expressed as

$$\begin{aligned} P_n &= \frac{1}{2} < \tilde{n}_1(t)\,\tilde{n}_1^*(t) > \\ &= \frac{1}{2} < \tilde{n}_2(t)\,\tilde{n}_2^*(t) > \\ &= \frac{1}{2} < \tilde{n}_3(t)\,\tilde{n}_3^*(t) >. \end{aligned} \tag{17}$$

By using the notations introduced previously, the complex envelopes $\tilde{x}_1(t)$, $\tilde{x}_2(t)$, and $\tilde{x}_2'(t)$ shown in Fig. 3 may be written as

$$\tilde{x}_1(t) = (1/\sqrt{2}) \left[\tilde{d}(t) + \sum_{m=1}^{M} \tilde{i}_m(t) + \tilde{n}_1(t) \right] \quad (18)$$

$$\tilde{x}_2(t) = (1/\sqrt{2}) \left[\tilde{d}(t) + \sum_{m=1}^{M} \tilde{i}_m(t-t_m) \cdot e^{-j\phi_m} + \tilde{n}_2(t) \right] \quad (19)$$

$$\tilde{x}_2'(t) = (1/\sqrt{2}) \left[\tilde{d}(t) + \sum_{m=1}^{M} \tilde{i}_m(t-2t_m) \cdot e^{-j2\phi_m} + \tilde{n}_3(t) \right]. \quad (20)$$

The coefficient $1/\sqrt{2}$ is multiplied due to the two-way power dividers.

From (10) and (16)–(20) it is apparent that the steady-state complex weights w_1, w_2, w_1', and w_2' are given by

$$w_1 = w_2^* = w_1' = w_2'^* = \frac{1}{2} \left[\sum_{m=1}^{M} (P_{im} - \beta_m) + P_n \right] \quad (21)$$

where

$$\beta_m \triangleq \frac{1}{2} < \tilde{i}_m(t)\, \tilde{i}_m^*(t-t_m) > e^{j\phi_m} \quad (m=1,\ldots,M). \quad (22)$$

Consequently the complex envelopes $\tilde{x}_3(t)$ and $\tilde{x}_4(t)$ at the second stage are expressed as follows:

$$\tilde{x}_3(t) = \tilde{D}(t) + \sum_{m=1}^{M} \tilde{I}_m(t) + \tilde{N}_1(t) \quad (23)$$

$$\tilde{x}_4(t) = \tilde{D}(t) + \sum_{m=1}^{M} \tilde{I}_m(t-t_m)\, e^{-j\phi_m} + \tilde{N}_2(t) \quad (24)$$

where

$$\tilde{D}(t) \triangleq (1/\sqrt{2})\, (w_1 + w_1^*)\, \tilde{d}(t) \quad (25)$$

$$\tilde{I}_m(t) \triangleq (1/\sqrt{2}) \left[w_1^*\, \tilde{i}_m(t) + w_1\, \tilde{i}_m(t-t_m) \cdot e^{-j\phi_m} \right] \quad (m=1,\ldots,M) \quad (26)$$

$$\tilde{N}_1(t) \triangleq (1/\sqrt{2}) \left[w_1^*\, \tilde{n}_1(t) + w_1\, \tilde{n}_2(t) \right] \quad (27)$$

$$\tilde{N}_2(t) \triangleq (1/\sqrt{2}) \left[w_1^*\, \tilde{n}_2(t) + w_1\, \tilde{n}_3(t) \right]. \quad (28)$$

Let R_{DD}' be the covariance matrix of the desired signal components in $\tilde{x}_3(t)$ and $\tilde{x}_4(t)$. Similarly let R_{NN}' be that of the noise components (the sum of the interference signals and internal noise). Then we have

$$R_{DD}' = \frac{1}{2} \begin{bmatrix} < \tilde{D}(t)\, \tilde{D}^*(t) > & < \tilde{D}(t)\, \tilde{D}^*(t) > \\ < \tilde{D}(t)\, \tilde{D}^*(t) > & < \tilde{D}(t)\, \tilde{D}^*(t) > \end{bmatrix} = \frac{1}{2} (w_1 + w_1^*)^2 \begin{bmatrix} P_d & P_d \\ P_d & P_d \end{bmatrix} \quad (29)$$

$$R_{NN}' = \begin{bmatrix} \nu & \zeta \\ \zeta^* & \nu \end{bmatrix} \quad (30)$$

where

$$\nu \triangleq \frac{1}{2} \left[\sum_{m=1}^{M} < \tilde{I}_m(t)\, \tilde{I}_m^*(t) > + < \tilde{N}_1(t)\, \tilde{N}_1^*(t) > \right] \quad (31)$$

$$\zeta \triangleq \frac{1}{2} \left[\sum_{m=1}^{M} < \tilde{I}_m(t)\, \tilde{I}_m^*(t-t_m) > e^{j\phi_m} + < \tilde{N}_1(t)\, \tilde{N}_2^*(t) > \right]. \quad (32)$$

Substituting (26)–(28) into (31) and (32) yields

$$\nu = \frac{1}{2} \left[2\, w_1 w_1^* \left(\sum_{m=1}^{M} P_{im} + P_n \right) + w_1 w_1 \sum_{m=1}^{M} \beta_m^* + w_1^* w_1^* \sum_{m=1}^{M} \beta_m \right] \quad (33)$$

$$\zeta = \frac{1}{2} \left[w_1 w_1 \left(\sum_{m=1}^{M} P_{im} + P_n \right) + 2\, w_1 w_1^* \sum_{m=1}^{M} \beta_m + w_1^* w_1^* \sum_{m=1}^{M} \gamma_m \right] \quad (34)$$

where

$$\gamma_m \triangleq \frac{1}{2} < \tilde{i}_m(t)\, \tilde{i}_m^*(t-2t_m) > e^{j2\phi_m} \quad (m=1,\ldots,M). \quad (35)$$

Because the weight controller 3 works in the same manner as the weight controllers 1 and 2, the steady-state complex weights w_3 and w_4 are given by

$$\begin{bmatrix} w_3 \\ w_4 \end{bmatrix} = \frac{1}{2} \begin{bmatrix} <\tilde{x}_4(t)\, \tilde{x}_4^*(t)> - <\tilde{x}_3(t)\, \tilde{x}_4^*(t)> \\ <\tilde{x}_3(t)\, \tilde{x}_3^*(t)> - <\tilde{x}_3^*(t)\, \tilde{x}_4(t)> \end{bmatrix} = \begin{bmatrix} \nu - \zeta \\ \nu - \zeta^* \end{bmatrix}. \quad (36)$$

From these results the output SINR is expressed as

$$\text{SINR} = [w_3^* \quad w_4^*]\, R_{DD}' \begin{bmatrix} w_3 \\ w_4 \end{bmatrix} \Big/ [w_3^* \quad w_4^*]\, R_{NN}' \begin{bmatrix} w_3 \\ w_4 \end{bmatrix}$$

$$= P_d (w_1 + w_1^*)^2 [2v - (\zeta + \zeta^*)] \Big/ [2 (v^2 - \zeta \zeta^*)] \quad (37)$$

where w_1 is given by (21).

Now we consider the directional pattern of the two-stage system. Let ξ be the angle relative to the broadside. The directional pattern for frequency f is expressed as

$$P(\xi,f) = \Big| (w_1^* + w_2^* e^{-j\mu(\xi,f)}) w_3^* + (w_1^* e^{-j\mu(\xi,f)} + w_2^* e^{-j2\mu(\xi,f)}) w_4^* \Big| = \Big| w_1^* + w_2^* e^{-j\mu(\xi,f)} \Big| \cdot \Big| w_3^* + w_4^* e^{-j\mu(\xi,f)} \Big| \quad (38)$$

where

$$\mu(\xi,f) \triangleq (2\pi f l \sin\xi)/c. \quad (39)$$

$|w_1^* + w_2^* e^{-j\mu(\xi,f)}|$ in (38) is the directional pattern realized by the complex weights w_1, w_2, w_1', and w_2' at the first stage. Similarly $|w_3^* + w_4^* e^{-j\mu(\xi,f)}|$ is that realized by the complex weights w_3 and w_4 at the second stage.

Here we consider that two narrowband interference signals are incident on the array. We assume that they may be regarded as CW signals with frequency f_c. Then (22) and (35) are rewritten as

$$\beta_m = P_{im} e^{j\phi_m} \qquad (m=1,2) \quad (40)$$

$$\gamma_m = P_{im} e^{j2\phi_m} \qquad (m=1,2). \quad (41)$$

Moreover we assume that $P_{i1} >> P_{i2}$, $P_{i2} >> P_n$, and $\phi_1 \neq 2n\pi$ hold. Then (21) is approximately given by

$$w_1 = w_2^* = w_1' = w_2'^* \simeq \frac{1}{2} P_{i1}(1 - e^{j\phi_1}). \quad (42)$$

Consequently we have

$$|w_1^* + w_2^* e^{-j\mu(\xi,f)}| \simeq 0 \qquad \text{for } \xi = \theta_1, f = f_c. \quad (43)$$

Expression (43) tells us that the first stage nulls the strong interference signal.

Expression (42) yields $\bar{I}_1(t) \simeq 0$. Then, by using (31), (32), (36), and $P_{i2} >> P_n$, the complex weights w_3, w_4 are given by

$$w_3 = w_4^* \simeq \frac{1}{2} |w_1^* + w_1 e^{-j\phi_2}|^2 \cdot P_{i2} \cdot (1 - e^{j\phi_2}). \quad (44)$$

Thus we have

$$|w_3^* + w_4^* e^{-j\mu(\xi,f)}| \simeq 0 \qquad \text{for } \xi = \theta_2, f = f_c. \quad (45)$$

This means that the second stage nulls the weak interference signal.

From these results it is seen that if two narrowband interference signals are widely separated in power level, the first and second stages reject the strong and weak signals, respectively. However, if $P_{i1} >> P_{i2}$ does not hold, the null at each stage is shifted from the interference arrival direction. Performance degradation is caused. More detailed considerations will be done later.

Now we consider a case where the interference signals may not be regarded as CW signals. We represent the power spectral density of each interference signal by $S_{im}(f)$ $(m=1,\ldots,M)$. Then

$$\frac{1}{2} < \bar{i}_m(t)\, \bar{i}_m^*(t-t_m) > = 2 \int_{-f_c}^{f_c} S_{im} \cdot (f+f_c) e^{j2\pi f t_m} df \qquad (m=1,\ldots,M) \quad (46)$$

holds. Thus the following equations are derived:

$$\beta_{im} = 2 e^{j\phi_m} \int_{-f_c}^{f_c} S_{im}(f + f_c) e^{j2\pi f t_m} df \qquad (m=1,\ldots,M) \quad (47)$$

$$\gamma_{im} = 2 e^{j2\phi_m} \int_{-f_c}^{f_c} S_{im}(f + f_c) e^{j4\pi f t_m} df \qquad (m=1,\ldots,M). \quad (48)$$

Calculating (37) and (38) by use of (47) and (48), we may obtain the output SINR and directional pattern for broadband interference signals.

C. Numerical Results

Numerical calculations were done for open-loop systems whose array elements are spaced a half-wavelength apart at the center frequency of the desired signal.

At first we consider a case where two CW interference signals are incident on the single-stage and two-stage systems. Fig. 4 shows the output SINR as a function of the power ratio (P_{i1} / P_{i2}) for several interference arrival angles θ_1, θ_2 for the case $P_d / (P_{i1} + P_{i2}) = -30$ dB, $P_d / P_n = 20$ dB. Fig. 4 also illustrates the output SINR which is realized by the three optimum complex weights placed behind the three array elements. The performance is computed from the full 3 by 3 matrix. As may be seen from Fig. 4, when both interference signals have almost the same power, i.e., $P_{i1} / P_{i2} \simeq 0$ dB, the two-stage system does not reveal such a superior performance over the single-stage system. And in this situation, the performance of the two-stage system is far below optimum. The reason for this is that the pattern nulls are shifted from the interference arrival directions as discussed in the previous subsection.

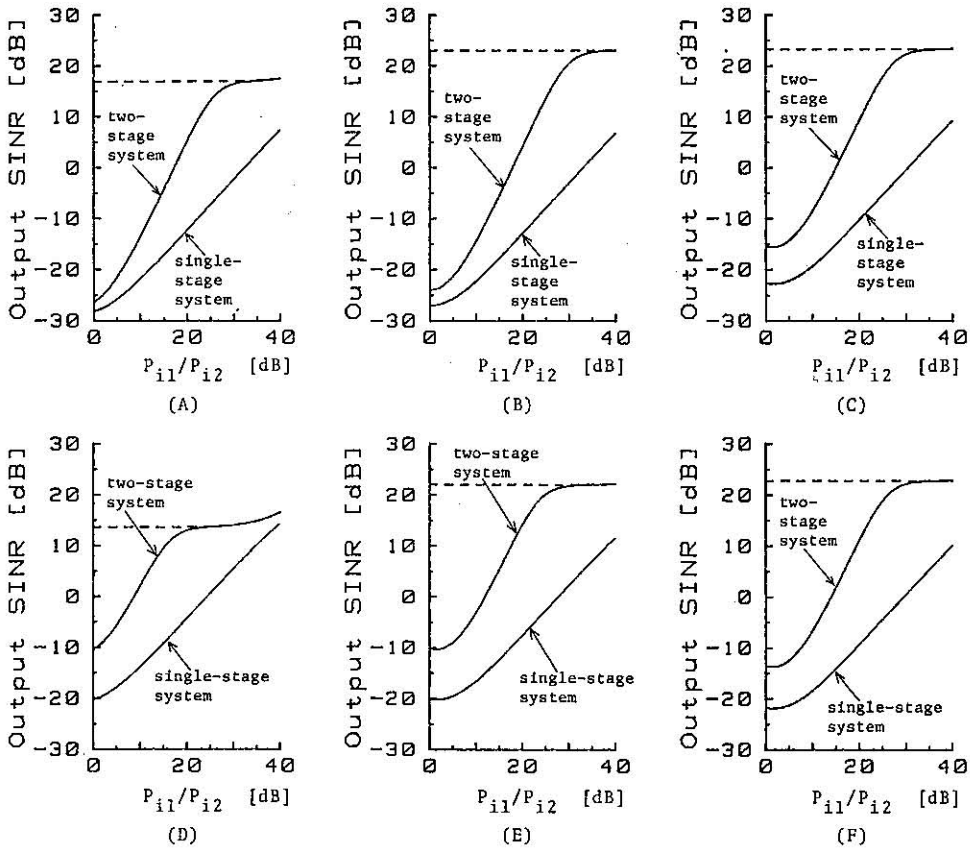

Fig. 4. Output SINR versus power ratio (P_{i1}/P_{i2}). Two CW interference signals are incident on open-loop system. Dotted lines show output SINR which is realized by three optimum complex weights placed behind three array elements. $P_d/(P_{i1}+P_{i2})=-30$ dB, $P_d/P_n=20$ dB. (A) $\theta_1=30°$, $\theta_2=-15°$. (B) $\theta_1=30°$, $\theta_2=-30°$. (C) $\theta_1=30°$, $\theta_2=-75°$. (D) $\theta_1=30°$, $\theta_2=15°$. (E) $\theta_1=30°$, $\theta_2=60°$. (F) $\theta_1=30°$, $\theta_2=75°$.

Fig. 5 shows typical examples of the directional pattern of the two-stage system for several values of P_{i1}/P_{i2}. These figures assume $\theta_1 = 30°$, $\theta_2 = -30°$, and $(P_{i1}+P_{i2})/P_n = 50$ dB. It is apparent that when $P_{i1}/P_{i2} \geqq 15$ dB, the nulls are pointed almost exactly toward both interference signals. However, when $P_{i1}/P_{i2} \leqq 10$

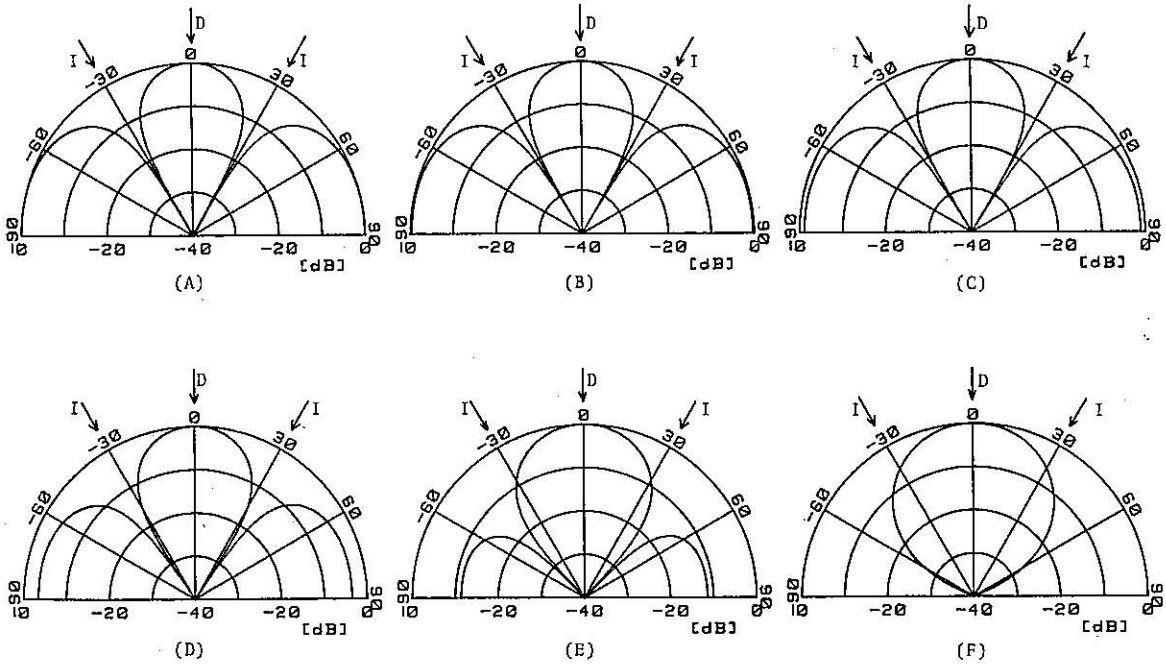

Fig. 5. Directional patterns of two-stage system. Interference signals are CW. D and I denote desired and interference signals, respectively. $(P_{i1}+P_{i2})/P_n=50$ dB, $\theta_1=30°$, $\theta_2=-30°$, $f=f_c$. (A) $P_{i1}/P_{i2}=30$ dB. (B) $P_{i1}/P_{i2}=20$ dB. (C) $P_{i1}/P_{i2}=15$ dB. (D) $P_{i1}/P_{i2}=10$ dB. (E) $P_{i1}/P_{i2}=5$ dB. (F) $P_{i1}/P_{i2}=0$ dB.

dB, the nulls are shifted from the proper directions. Thus it may be said that if CW interference signals are much stronger than the internal thermal noise and if there is a power ratio of more than 15 dB between the CW interference signals, a multiple-stage system may point the nulls toward them almost exactly. Although the steady-state performance of the multiple-stage system depends on the noise environment, we think that in many cases the system may suppress the interference signals satisfactorily. The reason for this is because multiple interference sources, if present, are likely to be at different power levels due to geographical distribution.

Now we consider the case where a single-interference signal with nonzero bandwidth is incident on the open-loop system. The power spectral density is assumed to be flat over the frequency range as shown in Fig. 6. We define the relative bandwidth r_B as

$$r_B \triangleq \Delta f / f_c. \tag{49}$$

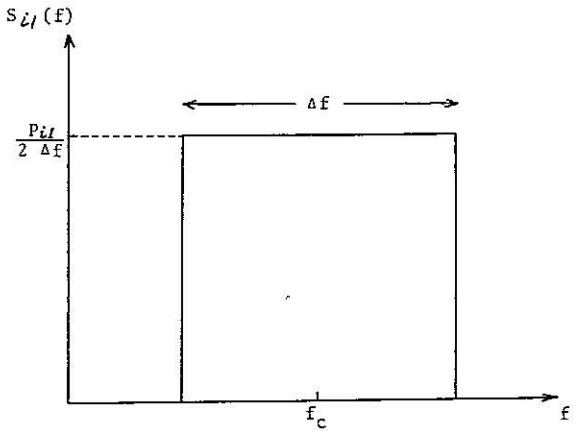

Fig. 6. Interference signal power spectral density.

Fig. 7 shows the output SINR as a function of r_B for several values of the interference arrival angle θ_1 for the case $P_d / P_{i1} = -30$ dB and $P_d / P_n = 20$ dB. It is seen that the two-stage system performs much better than the single-stage system except when the interference signal is near the desired signal at broadside.

Fig. 8 illustrates the effect of the relative bandwidth on the directional pattern of the two-stage system. These figures assume $\theta_1 = 30°$, $P_{i1} / P_n = 50$ dB, and $f = f_c$. Two nulls are gathered as the bandwidth of the interference signal becomes wider. At two percent or higher bandwidths, two nulls are formed coincidently. Consequently a broad null is formed toward the interference signal. This is the reason why the two-stage system has an excellent ability to reject a broadband interference signal.

The output SINR of the two-stage system on which two interference signals are incident is shown in Fig. 9 as a function of r_B. We assume that both interference signals have flat band-limited power spectral densities as shown in Fig. 6. As may be seen from these figures, the degradation of the output SINR due to interference band-

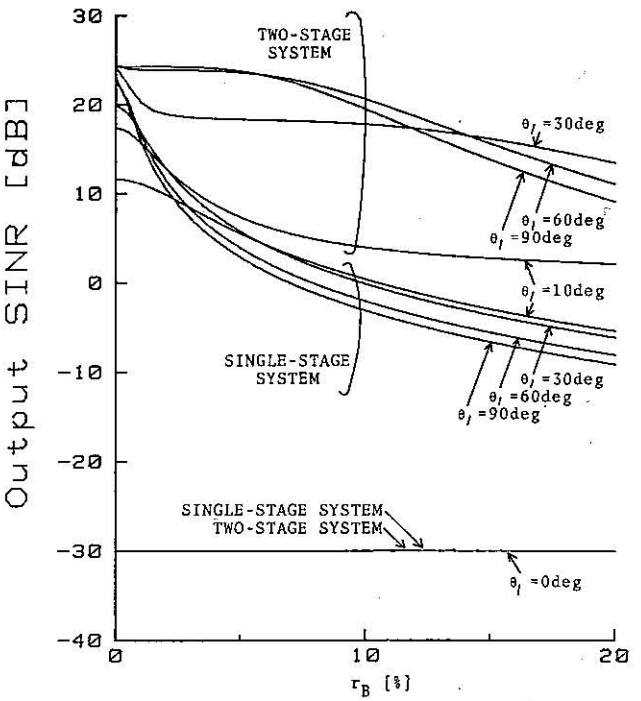

Fig. 7. Output SINR versus relative bandwidth. Single interference signal with flat band-limited power spectral density is incident on open-loop system. $P_d/P_{i1} = -30$ dB, $P_d/P_n = 20$ dB.

widths depends on the interference arrival angles θ_1, θ_2, and the power ratio P_{i1} / P_{i2}. Generally the larger the power ratio is, the more substantial the degradation is.

IV. COMPUTER SIMULATION RESULTS

We developed a computer program which simulates the open-loop systems. The output SINR was calculated by using (6) or (37). We assume that array elements are spaced a half-wavelength apart at the center frequency of the desired signal. We represent a unit of time as TU (time unit). For example 1 TU denotes 1 ms.

Signal parameters used in the simulation are shown in Tables I through IV.

The desired signal is assumed to be a biphase modulated signal [11]. Each modulated phase is statistically independent on different bit intervals and is 0 or π with equal probability. We represent the length of the bit interval by T_b.

For Cases 1 through 5 the interference signal is assumed to be a CW signal. For Cases 6 through 8 it is assumed to consist of plural (5 or 9) uniform amplitude and random phase sinusoidal waves, which have equally spaced discrete spectral lines as shown in Fig. 10. We consider that the latter signal is a broadband signal with relative bandwidth $\Delta f / f_c$.

We assume that the internal thermal noise is a white Gaussian wave.

The time constant τ of the first-order low-pass filters must be much larger than the length of bit interval T_b to such an extent that the complex weights do not interact with the desired signal modulation. Here τ is 0.1 and 1

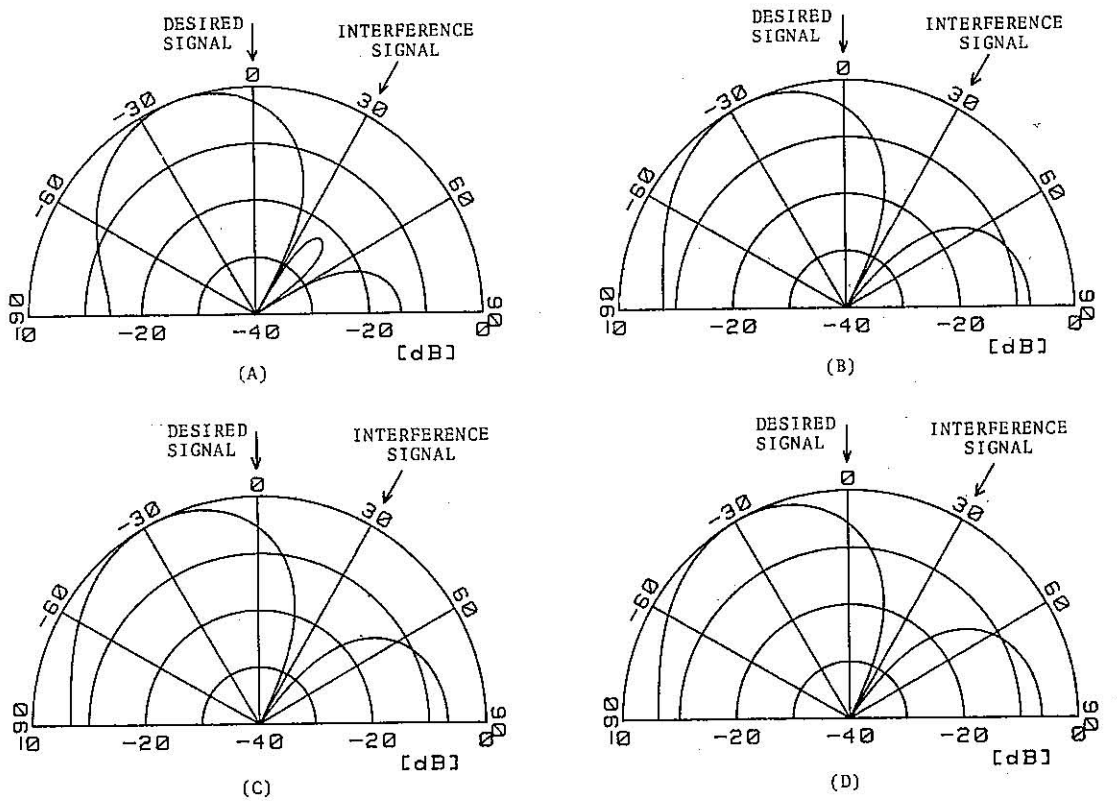

Fig. 8. Directional patterns of two-stage system. Single interference signal with flat band-limited power spectral density is incident on system. $P_{i1}/P_n = 50$ dB, $\theta_1 = 30°$, $f = f_c$. (A) $r_B = 1$ percent. (B) $r_B = 2$ percent. (C) $r_B = 3$ percent. (D) $r_B = 5$ percent.

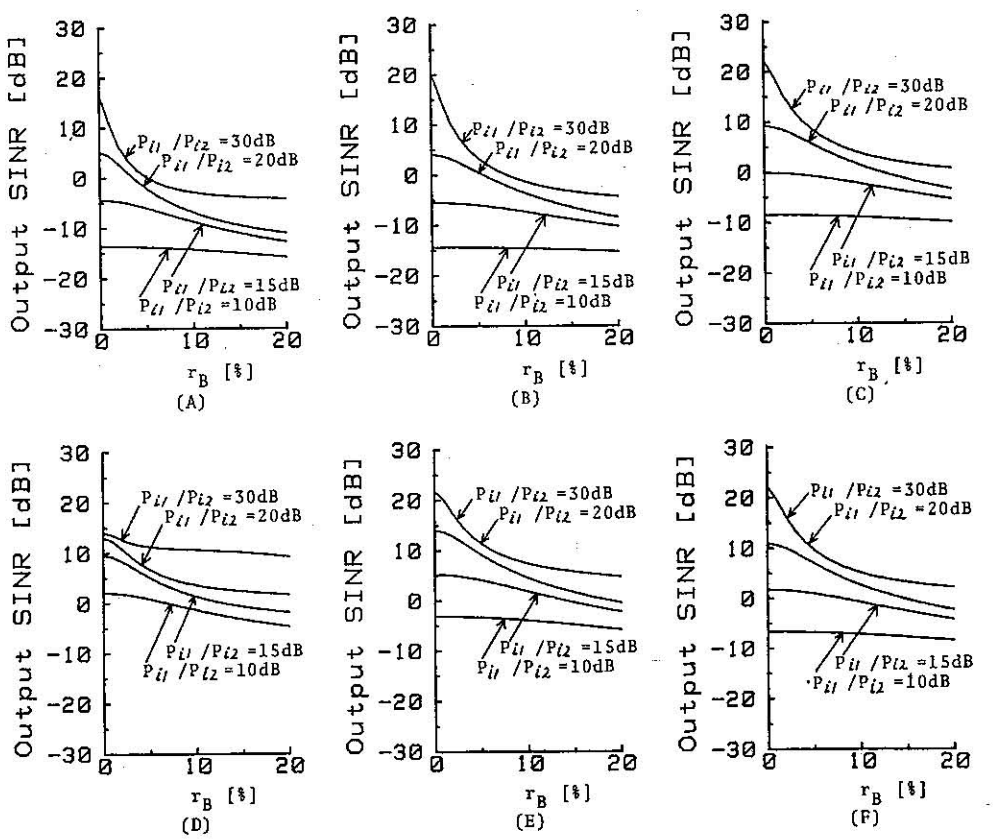

Fig. 9. Output SINR of two-stage system versus relative bandwidth. Two interference signals with flat band-limited power spectral density are incident on system. $P_d/(P_{i1}+P_{i2}) = -30$ dB, $P_d/P_n = 20$ dB. (A) $\theta_1 = 30°$, $\theta_2 = -15°$. (B) $\theta_1 = 30°$, $\theta_2 = -30°$. (C) $\theta_1 = 30°$, $\theta_2 = -75°$. (D) $\theta_1 = 30°$, $\theta_2 = 15°$. (E) $\theta_1 = 30°$, $\theta_2 = 60°$. (F) $\theta_1 = 30°$, $\theta_2 = 75°$.

TABLE I
Signal Parameters Used in Simulation (1)

		Case 1	Case 2
Desired Signal	Waveform	BPSK Wave	
	Carrier Frequency	200,000 Cycle/TU	
	T_b	0.01 TU	
Interference Signal	Waveform	C W	
	Frequency	200,005 Cycle/TU	
	P_d/P_{il}	-30 dB	-10 dB
	θ_1	30 deg	
Internal Thermal Noise	Waveform	White Gaussian Wave	
	P_d/P_n	20 dB	

TABLE II
Signal Parameters Used in Simulation (2)

		Case 3	Case 4	Case 5
Desired Signal	Waveform	BPSK Wave		
	Carrier Frequency	200,000 Cycle/TU		
	T_b	0.01 TU		
Interference Signal #1	Waveform	C W		
	Frequency	200,005 Cycle/TU		200,000.6 Cycle/TU
	P_d/P_{il}	-30 dB		
	θ_1	60 deg		
Interference Signal #2	Waveform	C W		
	Frequency	199,900 Cycle/TU		199,999.4 Cycle/TU
	P_d/P_{i2}	-10 dB	-20 dB	-10 dB
	θ_2	30 deg		
Internal Thermal Noise	Waveform	White Gaussian Wave		
	P_d/P_n	20 dB		

TU which are 10 and 100 times of T_b (0.01 TU), respectively.

Figs. 11 and 12 show the convergence results for the single-stage system and for Cases 1 and 2, respectively. Dotted lines indicate the steady-state SINR which is calculated on the assumption that there is no weight jitter. As may be seen from these curves, the output SINR converges at several times τ. The difference between Cases 1 and 2 is that of the interference signal power. A comparison of Fig. 11 with Fig. 12 shows that the convergence rate of the open-loop system is independent of the interference signal power. This is one of the advantages of the open-loop system.

Fig. 13 shows the convergence results for the two-stage system and for Cases 3 and 4. From Figs. 11

TABLE IV
Signal Parameters Used in Simulation (4)

		Case 8
Desired Signal	Waveform	BPSK Wave
	Carrier Frequency	20,000 Cycle/TU
	T_b	0.01 TU
Interference Signal #1	Waveform	5 Sinusoidal Waves
	Center Frequency	20,000.5 Cycle/TU
	P_d/P_{il}	-30 dB
	θ_1	60 deg
	Relative Bandwidth	3 %
Interference Signal #2	Waveform	5 Sinusoidal Waves
	Center Frequency	19,990 Cycle/TU
	P_d/P_{i2}	-10 dB
	θ_2	30 deg
	Relative Bandwidth	3 %
Internal Thermal Noise	Waveform	White Gaussian Wave
	P_d/P_n	20 dB

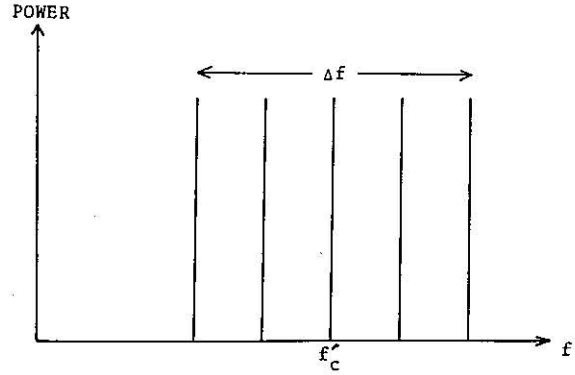

Fig. 10. Interference signal power spectrum having equally spaced uniform amplitude spectral lines.

TABLE III
Signal Parameters Used in Simulation (3)

		Case 6	Case 7
Desired Signal	Waveform	BPSK Wave	
	Carrier Frequency	20,000 Cycle/TU	
	T_b	0.01 TU	
Interference Signal	Waveform	5 Sinusoidal Waves	9 Sinusoidal Waves
	Center Frequency	20,000.5 Cycle/TU	
	P_d/P_{il}	-30 dB	
	θ_1	60 deg	
	Relative Bandwidth	3 %	6 %
Internal Thermal Noise	Waveform	White Gaussian Wave	
	P_d/P_n	20 dB	

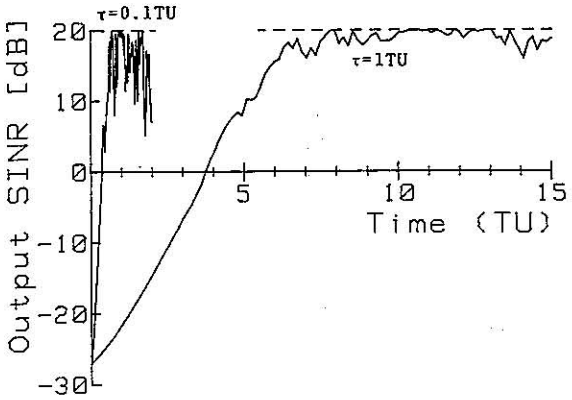

Fig. 11. Output SINR of single-stage system versus time (simulation results) (Case 1).

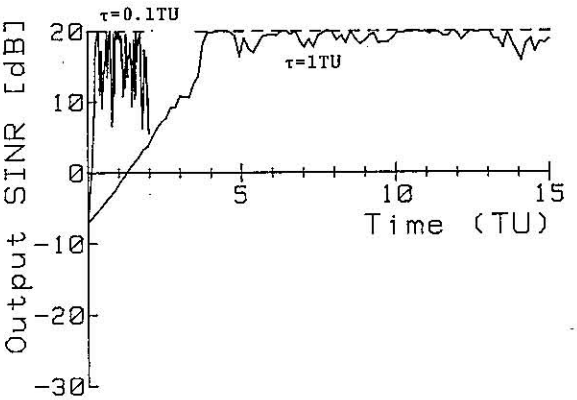

Fig. 12. Output SINR of single-stage system versus time (simulation results) (Case 2).

through 13 it is apparent that the convergence rate of the two-stage system is not essentially different from that of the single-stage system. As may be seen by comparing the results for Case 3 with those for Case 4, although the steady-state SINR depends on the ratio of the two interference signal powers, the convergence rate is independent of it. This is another advantage of the open-loop system, because the convergence rate of a conventional system with a feedback-loop becomes very slow when two interference signals are widely separated in power level. It is also seen that the output SINR is occasionally

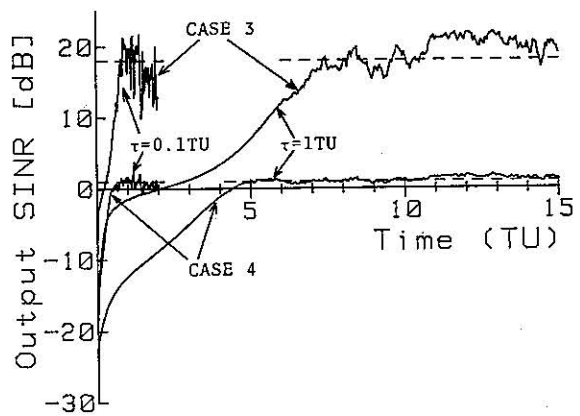

Fig. 13. Output SINR of two-stage system versus time (simulation results) (Cases 3 and 4).

better than the steady-state value, which is obtained on the assumption that there is no weight jitter. The reason for this is as follows. As discussed in the previous section, in a case where two interference signals are incident on the two-stage system, the formed nulls are more or less shifted from the interference arrival directions. Due to weight jitter these nulls are occasionally pointed to the interference signals exactly. This improves the output SINR.

If the frequencies of two CW interference signals are extremely close, a periodic ripple is seen in the steady-state output SINR as shown in Fig. 14. The reason for

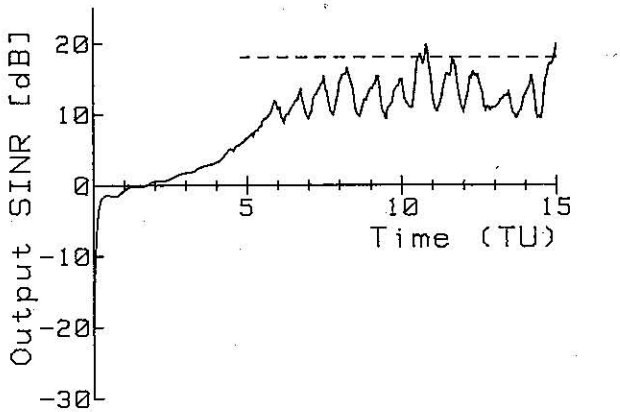

Fig. 14. Output SINR of two-stage system versus time (simulation results) (Case 5, $\tau = 1$ TU).

this is that the beat component of the two CW interference signals is not reduced sufficiently by the low-pass filters. Tables V and VI show 1) the average steady-state output SINR obtained from the simulation, 2) the steady-state output SINR calculated on the assumption that there is no weight jitter, and 3) the degradation of the steady-state output SINR due to the weight jitter. The average values are obtained from averaging about 10 000 data after time 10τ. As may be seen from these tables, the larger τ is, the less pronounced the degradation is due to the weight jitter. It is interesting that the average output SINR is occasionally improved in the two-stage system due to weight jitter. As shown later, in a case where the interference signal has a nonzero bandwidth, the degradation due to the weight jitter is less pronounced than the CW interference signal case. It may be said that if $\tau \geqq 10T_b$, the effect of the weight jitter is not so pro-

TABLE V
Effects of Weight Jitter on Steady-State Output SINR (1)

	Case 1		Case 2	
τ	0.1 TU	1.0 TU	0.1 TU	1.0 TU
Average Steady-State Output SINR (Simulation Results)	16.0 dB	18.9 dB	16.0 dB	18.9 dB
Steady-State Output SINR (Weight Jitter Is Absent.)	20.0 dB	20.0 dB	20.0 dB	20.0 dB
Degradation of Steady-State Output SINR due to Weight Jitter	4.0 dB	1.1 dB	4.0 dB	1.1 dB

TABLE VI
Effects of Weight Jitter on Steady-State Output SINR (2)

	Case 3		Case 4		Case 5
τ	0.1 TU	1.0 TU	0.1 TU	1.0 TU	1.0 TU
Average Steady-State Output SINR (Simulation Results)	17.6 dB	19.2 dB	1.1 dB	1.1 dB	16.0 dB
Steady-State Output SINR (Weight Jitter Is Absent.)	18.0 dB	18.0 dB	1.0 dB	1.0 dB	18.1 dB
Degradation of Steady-State Output SINR due to Weight Jitter	0.4 dB	-1.2 dB*	-0.1 dB*	-0.1 dB*	2.1 dB

*Average steady-state output SINR is improved due to weight jitter.

nounced except when the frequencies of plural narrowband interference signals are extremely close as in Case 5.

Convergence results for Cases 6 and 7 are shown in Fig. 15 and 16, respectively. In Figs. 11, 15, and 16 it is apparent that the convergence rate does not essentially depend on the bandwidth of an interference signal. This is an advantage of the open-loop system, because the convergence rate of the conventional system with a feedback-loop is highly dependent on the bandwidth of an interference signal. From these curves it is also apparent that if the interference signal has a nonzero bandwidth, the weight jitter has less effect on the steady-state output SINR than for the CW interference case.

Fig. 17 shows the convergence results for Case 8 and for the two-stage system. By comparing Fig. 17 with Fig. 13 we may see that although the output steady-state SINR depends on the bandwidth of two interference signals, the transient behaviors are independent of it.

From these results it may be concluded that the convergence rate of the analog open-loop adaptive-array system is independent of the noise environment. It is determined by the time constant of the low-pass filters. For the single-stage and two-stage systems, the output SINR converges at several times the time constant.

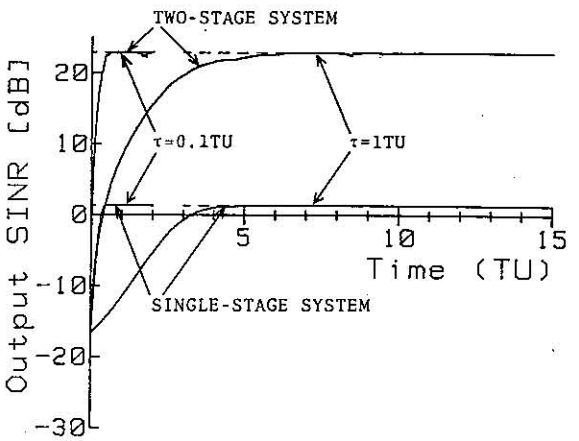

Fig. 16. Output SINR versus time (simulation results) (Case 7).

V. CONCLUSIONS

It has been shown that the analog open-loop adaptive-array system presented here has some advantages over conventional adaptive arrays regarding transient behaviors. First, the convergence rate of the open-loop system is essentially independent of the noise environment. It is determined by the time constant of the low-pass filters included in the system. From the simulation results the output SINR converges at several times the time constant. Hence it is possible to know the convergence time a

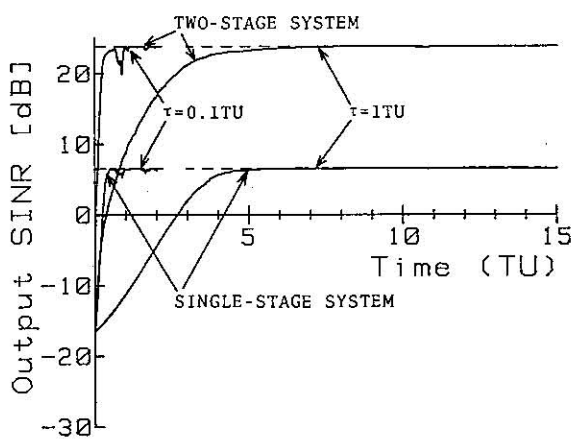

Fig. 15. Output SINR versus time (simulation results) (Case 6).

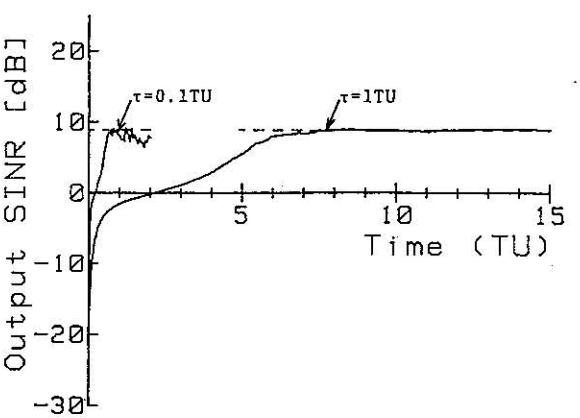

Fig. 17. Output SINR of two-stage system versus time (simulation results) (Case 8).

priori. Second, because the system consists of analog circuits, the convergence time is not limited by processing time involving digital logic components. Finally, the system is unconditionally stable. Thus, however small the time constant may be, the complex weights by no means diverge. This means that the open-loop system may provide a very rapid convergence rate.

Satisfactory steady-state performance is obtained in a case where a single interference signal exists in the field. When two or more interference signals are incident on the open-loop system, the steady-state performance depends on the noise environment. It may be concluded that the open-loop system is very useful when we have a single interference signal in the environment and very rapid interference protection is required.

REFERENCES

[1] Widrow, B., et al. (1967)
Adaptive antenna systems.
Proceedings of the IEEE, Dec. 1967, *55*, 2143-2159.

[2] Applebaum, S.P. (1976)
Adaptive arrays.
IEEE Transactions on Antennas and Propagation, Sept. 1976, *AP-24*, 585-593.

[3] Brennan, L.E., and Reed, I.S. (1973)
Theory of adaptive radar.
IEEE Transactions on Aerospace and Electronic Systems, Mar. 1973, *AES-9*, 237-252.

[4] White, W.D. (1976)
Cascade preprocessors for adaptive antennas.
IEEE Transactions on Antennas and Propagation, Sept. 1976, *AP-24*, 670-684.

[5] Compton, R.T., Jr. (1980)
Improved feedback loop for adaptive arrays.
IEEE Transactions on Aerospace and Electronic Systems, Mar. 1980, *AES-16*, 159-168.

[6] Reed, I.S., Mallett, J.D., and Brennan, L.E. (1974)
Rapid convergence rate in adaptive arrays.
IEEE Transactions on Aerospace and Electronic Systems, Nov. 1974, *AES-10*, 853-863.

[7] Horowitz, L.L., et al. (1979)
Controlling adaptive antenna arrays with the sample matrix inversion algorithm.
IEEE Transactions on Aerospace and Electronic Systems, Nov. 1979, *AES-15*, 840-847.

[8] Kretschmer, F.F., Jr., and Lewis, B.L. (1978)
A digital open-loop adaptive processor.
IEEE Transactions on Aerospace and Electronic Systems, Jan. 1978, *AES-14*, 165-171.

[9] Davies, D.E.N. (1967)
Independent angular steering of each zero of the directional pattern for a linear array.
IEEE Transactions on Antennas and Propagation, Mar. 1967, *AP-15*, 296-298.

[10] White, W.D. (1978)
Adaptive cascade networks for deep nulling.
IEEE Transactions on Antennas and Propagation, May 1978, *AP-26*, 396-402.

[11] Rodgers, W.E., and Compton, R.T., Jr. (1979)
Adaptive array bandwidth with tapped delay-line processing.
IEEE Transactions on Aerospace and Electronic Systems, Jan. 1979, *AES-15*, 21-28.

Yasutaka Ogawa was born in Sapporo, Japan, in 1950. He received the B.S., M.S., and Ph.D. degrees in electronic engineering from Hokkaido University, Sapporo, in 1973, 1975, and 1978.

Since 1979 he has been with Hokkaido University, where he is presently an Associate Professor of Electronic Engineering. His special interests are in adaptive-array antennas, standard frequency and time dissemination using a broadcasting satellite, and digital communication systems.

Dr. Ogawa is a member of the Institute of Electronics and Communication Engineers of Japan.

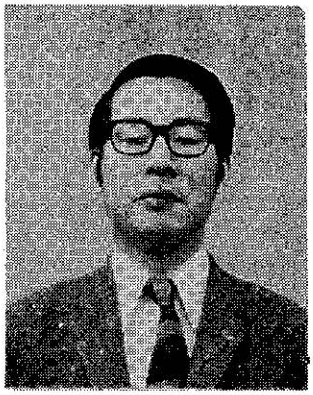

Kiyohiko Itoh was born in Sapporo, Japan, in 1939. He received the B.S.E.E. degree in 1963, the M.S. degree in 1965, and Ph.D. degree in 1973, all from Hokkaido University, Sapporo. Since 1965 he has been on the faculty of engineering at Hokkaido University, where he is a Professor of Electronic Engineering. From 1970 to 1971 he was with the department of electrical and computer engineering, Syracuse University, Syracuse, NY, as a Research Associate, on leave from Hokkaido University. His special interests are in electromagnetic radiation, standard frequency and time dissemination using a broadcasting satellite, wave optics, mobile radio communications, and the Solar Power Satellite.

Dr. Itoh is a member of the Institute of Electronics and Communication Engineers of Japan and also an international coordinator of the Antennas and Propagation Society of the IEEE.

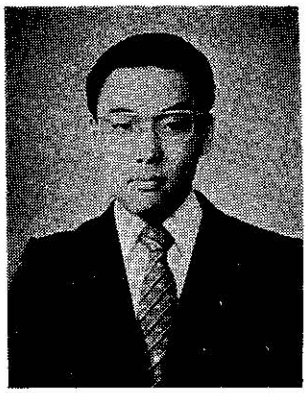

Manabu Ohmiya was born in Sapporo, Japan, in 1957. He received the B.S. degree in electronic engineering from Hokkaido University, Sapporo, in 1981.

At present he is a graduate student in electronic engineering at Hokkaido University. His current research interests include adaptive antennas, signal processing, and information theory.

Mr. Ohmiya is a member of the Institute of Electronics and Communication Engineers of Japan.